Melt Rheology of Blends of Semicrystalline Polymers. I. Degradation and Viscosity of Poly(ethylene Terephthalate)–Polyamide-6,6 Mixtures

L. A. UTRACKI, A. M. CATANI, and G. L. BATA, *National Research Council of Canada, Industrial Materials Research Institute, 750 Bel-Air, Montreal, Quebec, H4C 2K3* and M. R. KAMAL and V. TAN, *McGill University of Chemical Engineering, Montreal, Quebec, H3A 2A7, Canada*

Synopsis

Melt rheology of poly(ethylene terephthalate)–polyamide-6,6, and their blends was studied between 240°C and 300°C, in capillary and rotational rheometers. The flow curves were determined in the range of rate shear from about 10^{-2} to 10^{5} (s^{-1}). The results indicate a considerable degree of compatibility, presence of associations between the two types of macromolecules, and cocrystallization. A new mechanism of flow for the blends has been proposed. The study also considers the kinetics of thermal degradation.

INTRODUCTION

The utilization of polymer blends and alloys is an increasingly important segment of the plastics industry. The commercial production of blends in 1983 is projected[1] to reach 600,000 tons. The advantages of blending and the resulting blend properties have been summarized in a series of recent reviews.[2–5] These suggest that most of the work done in this field is related either to the material of commercial importance (viz., rubber modified polystyrene, poly(phenylene oxide)/polystyrene, ABS, PVC blends, etc.) or to compatible polymer mixtures.

Compatibility in most cases[4] leads to additivity of properties. Synergistic compatible mixtures tend to be rare. On the other hand, the compatible systems can be theoretically treated in an exact manner,[6] and their properties may be computed from those determined for the pure polymers. A much greater challenge and potentially greater rewards might be found in the field of incompatible polymer blends.[2,3] In this case, the final properties will be determined by those of the pure polymers, geometrical arrangements of the two phases, their morphology, the extent of interpenetration, and the nature of the interface. In this first part of the series we wish to report on the preliminary results of viscosity measurements of poly(ethylene terephthalate) (PET) blends with polyamide-66 (PA).

Journal of Applied Polymer Science, Vol. 27, 1913–1931 (1982)
 CCC 0021-8995/82/061913-19$02.90

TABLE I
Properties of the Resins (As Quoted in Commercial Literature)

Commercial name: Symbol:	Kodapak 7352 PET	Zytel 42 PA 42	Zytel 101 PA 101
M_w	55,000	(36,000)[a]	(15,000)[a]
M_w/M_n	2.2	—	—
Melting point (°C)	<257	258	255
"Softening" point (°C)	245	—	—
Melt viscosity at 275°C (poise)	—	25,000	1,300

[a] Values estimated from the melt viscosity[7] at 275°C.

EXPERIMENTAL

Materials and Sample Preparation

Three commercial resins, listed in Table I, were used. Prior to blending, PET was dried for 24 h at 135°C and PA for the same period but at 85°C. Weighed amounts of the resins were tumble-mixed in a double-cone blender for 5 min and immediately loaded into the hopper of a Metalmeccanica-6SRE reciprocating screw injection molding machine. The temperatures of the three zones of the barrel were kept at 280°C, 260°C, and 200°C. The moldings were ground in a granulator Alsteel (with $^3/_{16}$-in. diameter holes) screen.

For capillary flow measurements, the granules (dried in a vacuum oven at 110°C for at least 18 h) were used directly. For the rotational rheometer, the dried granules were pressed into 1.5-mm-thick discs of a diameter equal to that of the testing fixtures. In order to compare the behavior of the blends with that of the pure polymers, the latter were processed in a similar fashion.

Table II shows the molecular weights of PET before and after processing. In the following text, reference to the pure resins implies results obtained with the processed samples.

MEASUREMENTS

The melting point T_m (°C) of all the samples was determined by differential scanning calorimetry (Perkin-Elmer DSC-1B). The instrument was calibrated prior to use at 20°C/min. The pressed and slowly cooled samples (the same as used in the rotational rheometer) were used.

The Rheometrics Mechanical Spectrometer, Model RMS-605, was used in the steady state (cone-and-plate) and dynamic (parallel-discs) modes with both 25- and 50-mm diameter testing fixtures. Compression molded samples having the desired diameter were stored in a vacuum oven at 110°C, until the time of the test. The measurements at 300°C and 290°C were carried out isothermally,

TABLE II
Molecular Parameters of PET before and after Processing (GPC Results)

	Before	After
Weight average (M_w)	1.72×10^5	1.49×10^5
Number average (M_n)	4.38×10^4	3.41×10^4
M_w/M_n	3.92	4.38
z-Average (M_z)	1.02×10^6	1.60×10^6

i.e., the test fixtures were preheated to the temperature of the measurements. For the lower test temperatures (280°C, 260°C, 240°C), the fixtures were preheated to 290°C; then, the sample was loaded, trimmed, and, subsequently, the temperature was adjusted to the desired level. The total waiting time (from the time of loading until the start of measurement), or the soak time, was kept at minimum, normally from 40 s to 3 min. The testing was carried out in a hot air medium inside an environmental chamber surrounding the test fixtures. Initial tests indicated that the decrease of viscosity with time (see below) was not significantly different if nitrogen was used instead of air. The remaining experimental and computational details followed standard procedures.[8]

The high shear rate ($\dot{\gamma} > 10^2\ s^{-1}$) viscosities were determined with the Instron Capillary Rheometer (ICR). The dried granular samples, stored in the vacuum oven at 110°C, were loaded into the preheated barrel. The isothermal viscosity was measured at 280°C and 300°C using dies of diameters d = 0.51 and 1.32 mm with a 90° entrance angle and a length-to-diameter ratio (L/d) = 40. The previously described procedure[9,10] was modified to permit at least two extrusions at the same crosshead speed from the same load, but with different residence times. This yielded information regarding degradation effects and made it possible to correct viscosity data for these effects.

In the initial part of the study, a series of experiments were performed using capillaries with L/d = 5, 10, 20, and 40. It was found that, in the full range of $\dot{\gamma}$, the Bagley correction did not exceed 5%. As a result, the correction was subsequently neglected.

RESULTS

Correlation of rheological data obtained from capillary and rotational rheometers is not always possible.[10] However, in order to obtain data over a broad range of shear rates, both types of measurement are usually needed. Similarly, numerical agreement of results obtained from steady-state and dynamic rheological measurements frequently poses problems.[11]

The RMS data reported below were collected in both the steady-state (0.04 rad cone-and-plate) and the dynamic (parallel discs) modes. In Figure 1, the isothermal, uncorrected data of the steady shear viscosity η (poise) as a function of the rate of shear $\dot{\gamma}$ (s^{-1}) and the dynamic viscosity η^* (poise) as a function of frequency ω (rad/s) are plotted for PET at 280°C. The dynamic measurements were carried out at ϵ = 60% strain, selected on the basis of strain scan (at ω = 1) as the optimum ϵ-value for the stability of the three dynamic functions: η^*, storage modulus G' (dyn/cm^2), and loss modulus G'' (dyn/cm^2). Since similar excellent agreement between dynamic and steady state data was found for the other samples of the series, there will be no distinction made between RMS viscosities η and η^* on the following graphs. (Unless otherwise stated, the units of η,η^*, G', and G$''$ will be the same throughout this manuscript as those indicated above.)

Thermal degradation of both PET and PA was a complicating factor in the rheological measurements. In order to correct the RMS data, each sample, at each temperature, was tested for as long as 40 min at ω = 1 and 10 with ϵ = 60%. These measurements permitted construction of the curves presented in Figure 2 for the temperatures T = 280°C and 300°C. For clarity, most of the points have been omitted.

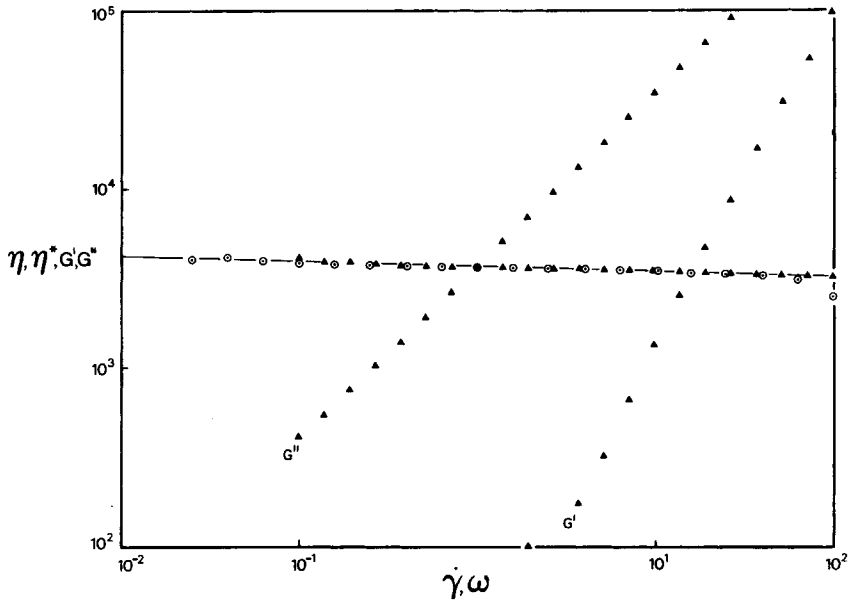

Fig. 1. Rheological properties of PET at 280°C. (⊙)η, RMS, cone-and-plate in steady; (▲)η^*, G', G'', ϵ = 60%, RMS, parallel disc in oscillation. Uncorrected data.

The isothermal logarithmic decrement of viscosity, D, was computed according to the following relationship:

$$D \equiv -10^3 \times (d \ln \eta^*/dt) \tag{1}$$

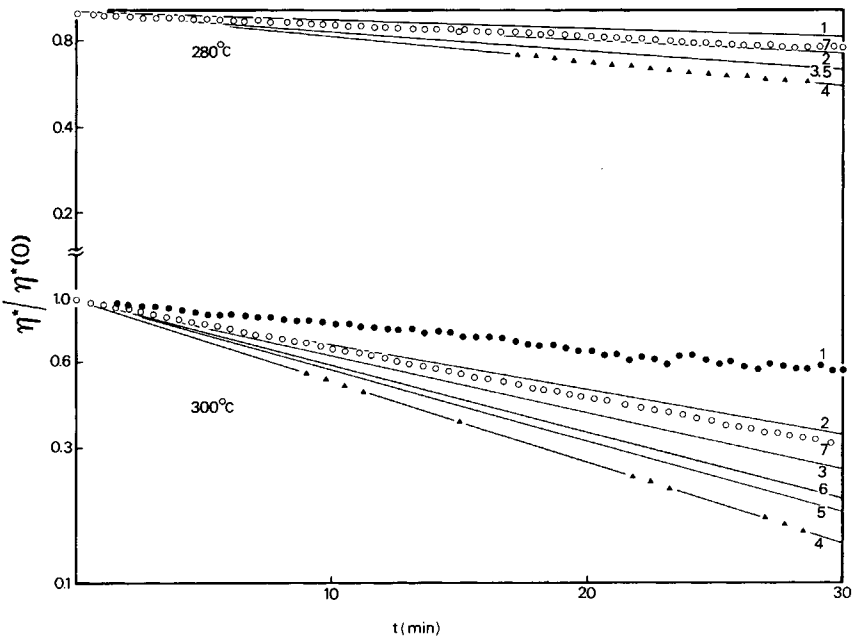

Fig. 2. Relative decrease of melt viscosities with time. RMS parallel disc at 280°C and 300°C; strain ϵ = 60%, frequency ω = 10 rad/s. For clarity most of the points are omitted. (1) PET; (2) B 2/1; (3) B 2/2; (4) B 2/3; (5) B 2/4; (6) B 2/5; (7) PA 42.

Dependence of this parameter on temperature is shown in Figure 3. A cross plot of D (interpolated values) as a function of PA concentration c (wt %) at T = 260°C, 280°C, and 300°C is presented in Figure 4. Here the values computed from ICR data are also included.

The dependencies shown in Figure 3 allow calculation of the apparent overall activation energy of the degradation process, E_D:

$$E_D \equiv R\ [d \ln D/d(1/T)] \tag{2}$$

The results are summarized in Table III and Figure 5.

In Figures 6–12 the isothermal viscosities η or η^* as functions of $\dot{\gamma}$ or ω are shown. For B 2/1–B 2/3, the values of η obtained from the ICR tend to be higher than those from RMS. It seems that for the samples containing low concentration of PA in PET, some wall effect takes place. Similar behavior was recently reported[12] for another pair of incompatible polymers: ethylene–propylene–1,4-hexadiene terpolymer (EPDM) with poly(vinylidene fluoride–co-hexafluro propylene) (Viton).

The Newtonian or "zero shear" viscosities, η_0 (determined from the horizontal part of the curves presented in Figs. 6–12), were employed to estimate the activation energy of flow, E_η:

$$E_\eta = R[d \ln \eta_0/d(1/T)] \tag{3}$$

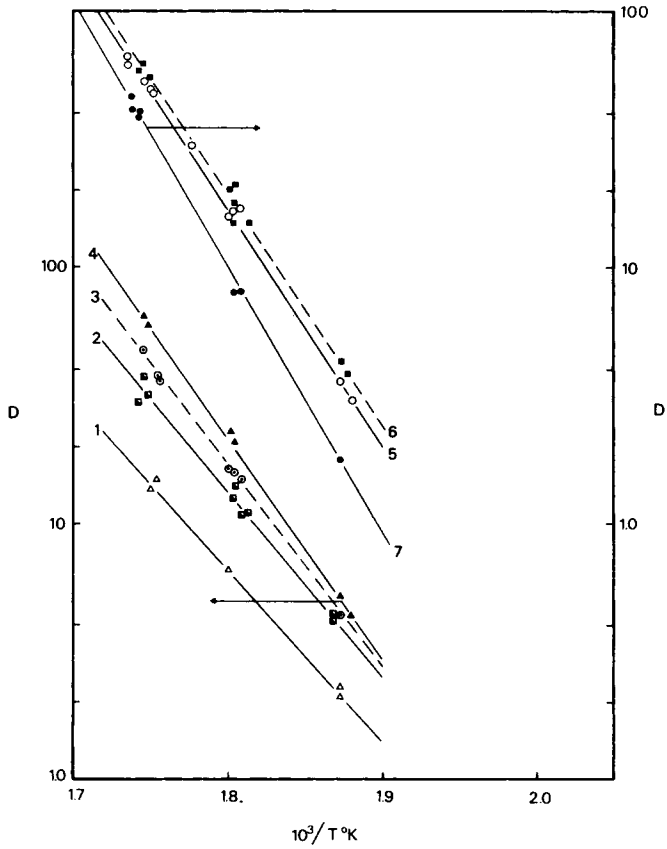

Fig. 3. Logarithmic decrement of viscosity as a function of temperature. Numbers refer to samples as in Figure 2.

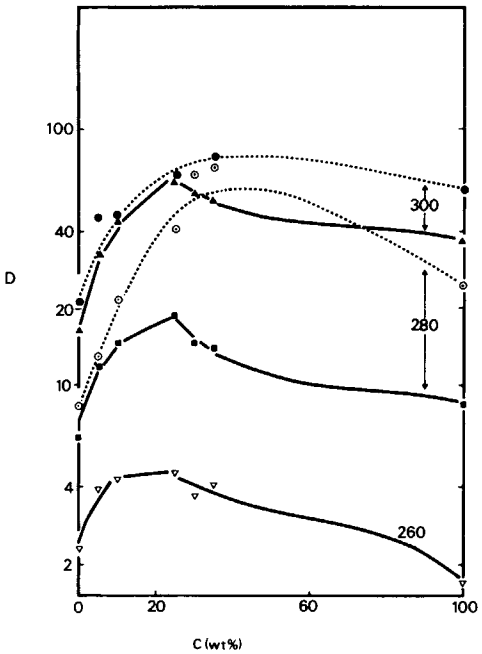

Fig. 4. Logarithmic decrement of viscosity as a function of PA content. (—) RMS: (▲) 300°C; (■) 280°C; (▽) 260°C. (·····) ICR: (●) 300°C; (⊙) 280°C.

The results are listed in Table III. The values for PA 101 and its blend with PET are also quoted under the "RMS" heading. For comparison, the E_η computed from ICR η's at 280°C and 300°C and at $\dot{\gamma} = 10^3$ (s^{-1}) are also listed. The concentration dependence of E_η is shown in Figure 13. A cross plot of η_0 (T = const) as a function of PA 42 content is presented in Figure 14. The data were interpolated from the Arrhenius plot ln η_0 vs. $1/T$.

In order to verify that the form of the η vs. c dependence is maintained at higher $\dot{\gamma}$, Figure 15 shows a plot: $\eta(\dot{\gamma}, T = \text{const})$ vs. c for higher shear rates. These are ICR data, with the exception of the $\dot{\gamma} = 100$ curves, where the values from RMS were also available.

Qualitatively, both Figures 14 and 15 give the same picture; i.e., in the full range of $\dot{\gamma}$ investigated here, the blends have lower viscosity than predicted by a simple additivity rule from the η's of pure polymers.

TABLE III
Activation Energies for PET/PA Blends (kcal/mol)

No.	Sample	PA content c (wt %)	$E_d \pm 2$	$E_\eta \pm 2$ RMS	$E_\eta \pm 2$ ICR
1	PET	0	30	9	11
2	B 2/1	5	33	17	15
3	B 2/2	10	37	21	19
4	B 2/3	25	40	20	22
5	B 2/4	30	43	21	21
6	B 2/5	35	40	19	21
7	PA 42	100	47	28	20
8	B 4/2[a]	25	38	8	13
9	PA 101	100	11	5	15

[a] This blend contains PA 101; the others are with PA 42.

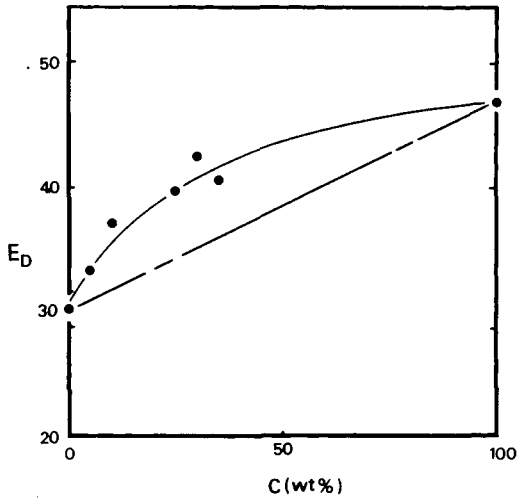

Fig. 5. Activation energy of the degradation (kcal/mol) as a function of PA content.

Figures 16 and 17 summarize the results of DSC scans of the pure polymers and of their blends. The data in Figure 16 are vertically shifted to allow direct comparison of the endothermic peak position. The melting temperature T_m determined from these data is plotted in Figure 17 as a function of composition. It can be seen that the DSC curves in Figure 16 return to a baseline at $T < 275°C$, i.e., the melting of the samples seems to be complete at 275°C.

In RMS, for samples B 2/4 and B 2/5 loaded and measured at 280°C, a hyperbolic type of curves (shown by black squares in Fig. 18) was consistently obtained. The same type of dependence was seen for 1–9-min waiting (soak) times at the loading temperatures 280°C and 285°C. However, once the loading temperature was increased to 290°C, the normal η vs. $\dot{\gamma}$ dependence was obtained.

Finally, to complete the "Results," a few words on the morphology of the molten blends. It was observed that at temperatures above the crystallization temperature B 2/1, containing 5% PA, was transparent and optically homogenous,

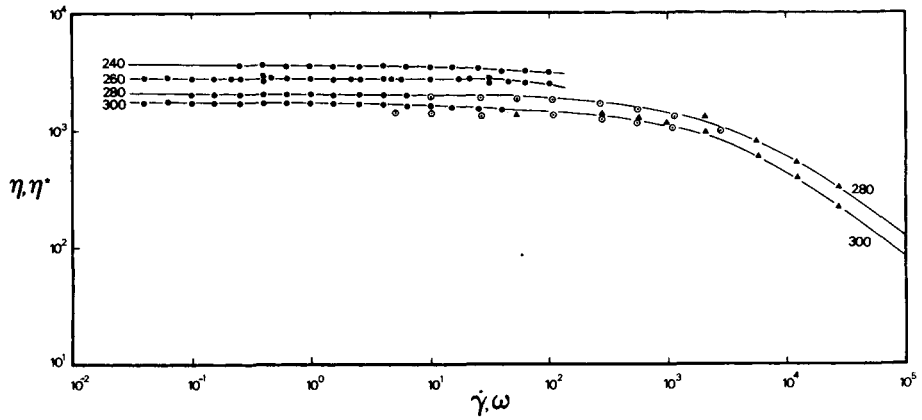

Fig. 6. Viscosities of PET at 240°C, 260°C, 280°C, and 300°C; (●)η,η^*, RMS; (⊙) ICR, L/d = 40, d = 1.32 mm, D = 0.052 in.; (▲) ICR, L/d = 40, d = 0.51, D = 0.020 in.

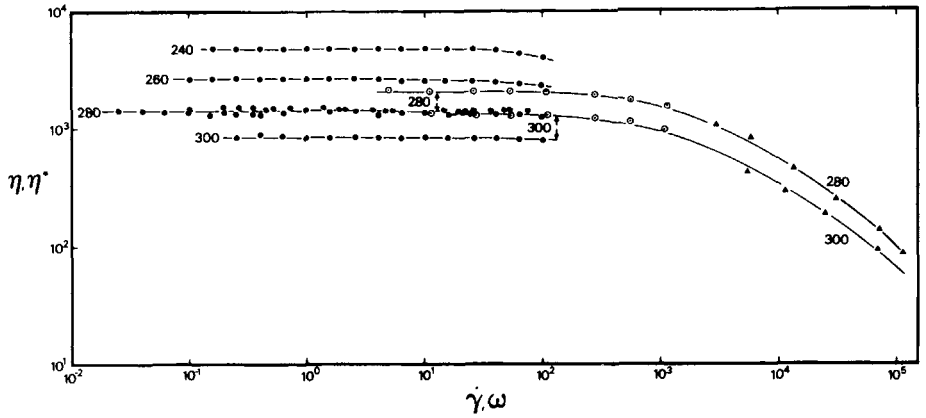

Fig. 7. Viscosities of B 2/1 at the four temperatures indicated. Symbols as in Figure 6.

indicating that if a phase separation does occur, the droplet size must be below 0.2 μm. All the other blends listed in Table III were opaque; i.e., independently of temperature they contained optically heterogeneous domains. The results of infrared multiple reflextion analysis showed that at least up to 30 wt % PA in the blend the continuous phase consisted of PET. This was confirmed by optical microscopy of quenched B 2/2–B 2/5 samples. Spherical domains 2–100 μm in diameter were observed. The number of these domains increased as c was raised.

DISCUSSION

In a recent review,[13] van Oene rightly stated that the rheology of polyblends shows a number of peculiarities which are difficult to understand. The general confusion is compounded by the fact that different authors evaluate the data in different ways. The simplest and the most straightforward set of data to analyze are those of the Newtonian region. Since this region for the present system extends over 2–3 decades of $\dot{\gamma}$, the η_0 values are well established, and they will be the main basis in the following discussion.

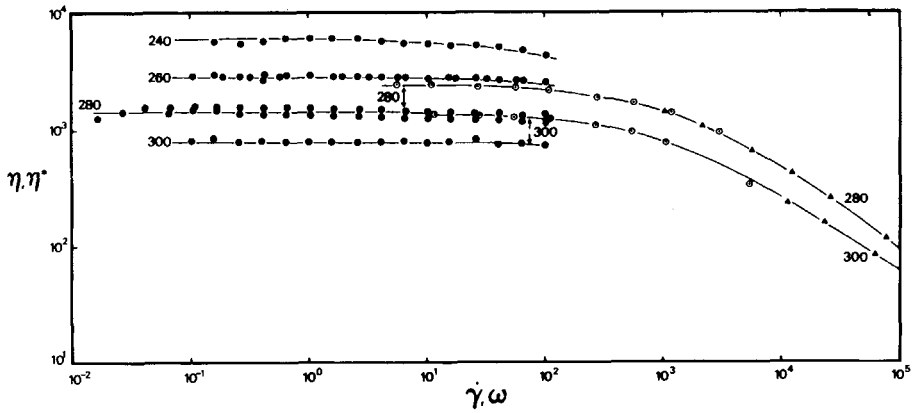

Fig. 8. Viscosities of B 2/2 at the four temperatures indicated. Symbols as in Figure 6.

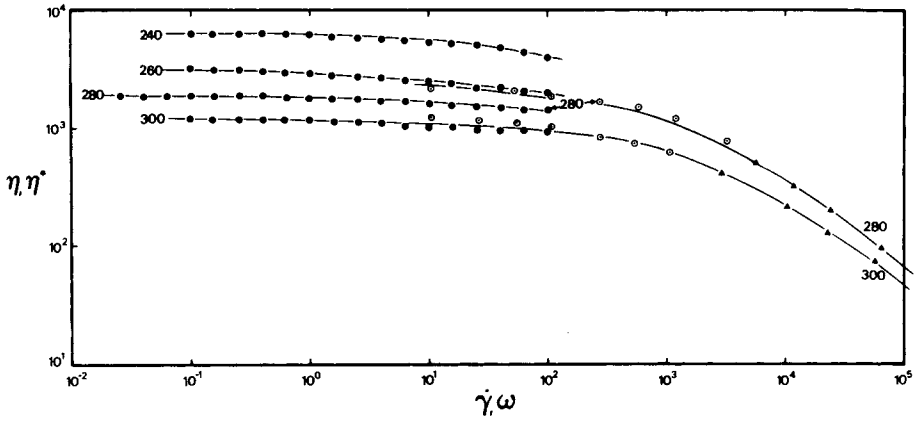

Fig. 9. Viscosities of B 2/3 at the four temperatures indicated. Symbols as in Figure 6.

Degradation

The data shown in Figure 2 for $\omega = 10$ (rad/s) represents equally well the blend behavior at shear rates $\dot{\gamma} \leq 10^3$ (s^{-1}), except for $\omega \leq 1$ data for B 2/5 and PA. In the latter case, oxidative degradation occurring at high temperatures and long exposure times gradually resulted in the formation of black resinous cake around the gap, which led to an increase in the apparent η^*.

The thermal degradation of the samples calculated from the curves exemplified by Figure 2 can be most conveniently discussed in terms of the parameters D and E_D. It is apparent that the degradation follows a first order kinetic equation in which the overall kinetic constant k_1 is proportional to D. This is in accord with the data published[14] on the thermal degradation of PET and the proposed mechanism of random chain scission. A similar mechanism seems to be true for PA and the blends. For PA, the random cleavage of C—N bond has been postulated.[15] It can be seen in Figure 4 that the rate of degration of the blends is higher than that of the pure polymers. It is also higher than values calculable from the simple additivity rule. Most likely, the acceleration is due to the initial

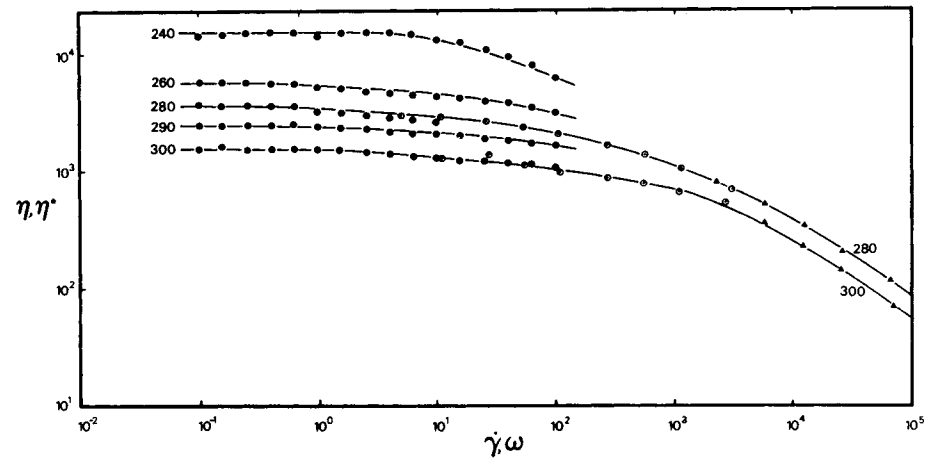

Fig. 10. Viscosities of B 2/4 at the five temperatures indicated. Symbols as in Figure 6.

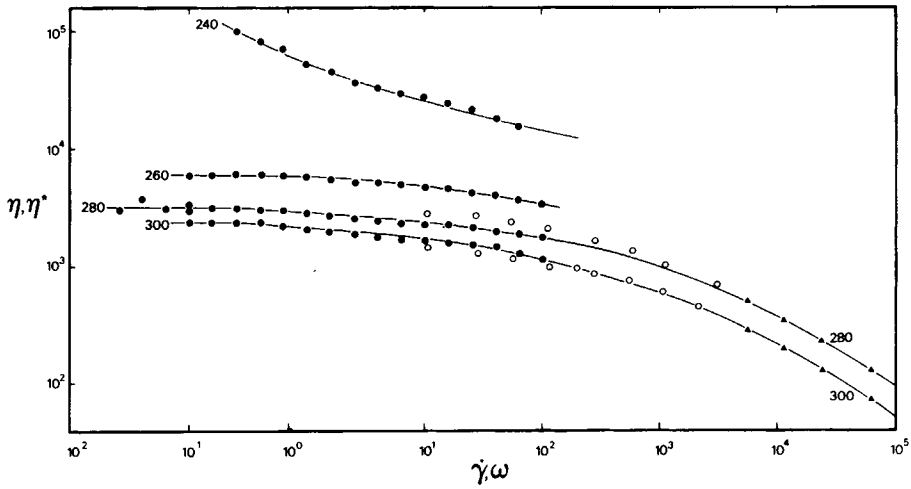

Fig. 11. Viscosities of B 2/5 at the four temperatures indicated. Symbols as in Figure 6.

catalytic effect of the amide groups on the degradation of PET, which in turn accelerates the decomposition of PA. It is interesting to note that the degradation rates in RMS and ICR are very comparable at 300°C but not at 280°C. In the latter case, the values of D, calculated from ICR data for samples with a higher PA content, are about 2.5 times higher. This may indicate an effect of shear degradation at the capillary wall.

The overall activation energy values of thermal degradation for the pure polymers are listed in Table IV. It can be seen that the E_D values quoted in the literature vary over a wide range (especially for PA). The values calculated in this work for PET and PA 42 are well within the range while that for PA 101 seems low. In Figure 5, the concentration dependence of E_D is shown. The curve is drawn according to the simplest interactive relation:

$$E_D = X_1E_1 + X_2E_2 + X_1X_2\Delta E \tag{4}$$

where X_i, E_i are the mole fraction and E_D for PA (subscript 1) and PET, respectively. The data can be fitted with error ±1.2 (kcal/mol) by employing a

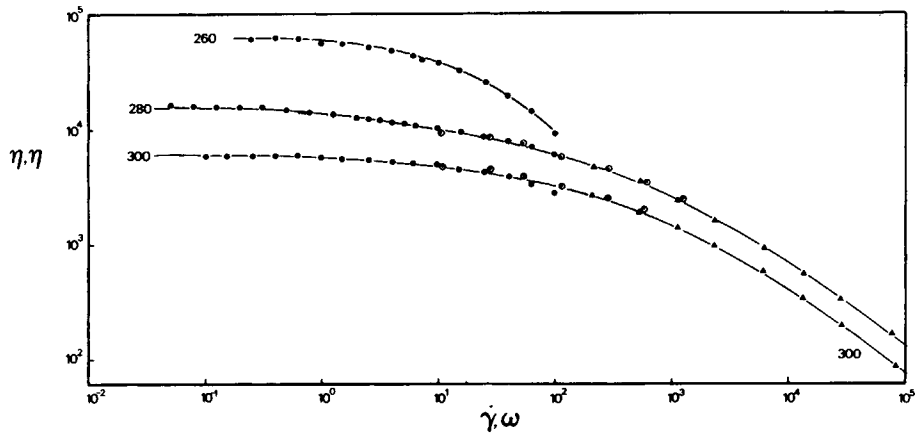

Fig. 12. Viscosities of PA at the three temperatures indicated. Symbols as in Figure 6.

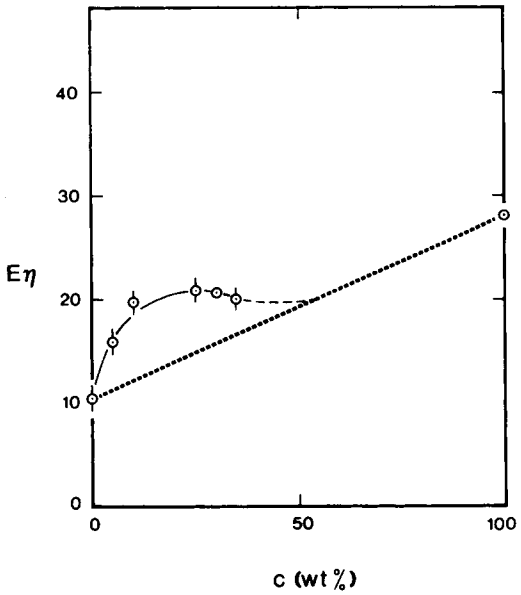

Fig. 13. Activation energy of the viscous flow (kcal/mol) as a function of PA content.

value for the interactive term ΔE = 20 (kcal/mol). This is a rather large synergistic effect.

Shear-Dependent Viscosities

The η vs. $\dot{\gamma}$ dependencies presented in Figures 6–12 span nearly 7 decades of $\dot{\gamma}$. The range of the Newtonian behavior was observed to be significantly larger for the pure polymers than for the blends. In the blends, transition from the Newtonian to a slightly pseudoplastic flow was observed at relatively low $\dot{\gamma}$ = 1 (s^{-1}), or at the shear stress $\sigma_{12} = 10^3$ (dyn/cm^2). In general, the transition from Newtonian behavior occurred at lower shear rates as c increased. One may interpret these results as follows. For PET the system is homogeneous, and the data can be approximated by a single theoretical dependence.[20] The initial dispersion of PA in the form of readily deformable droplets generates a series of shear-dependent structures, each with its own value of the characteristic "zero-shear" viscosity. As c increases, so does the extent of this structural deformation of the dispersed phase; the deviation from the Newtonian behavior occurs at lower $\dot{\gamma}$ even when η_0 is lowered. For $c \geq 30\%$, this effect is no longer visible—the droplets in this zone are most likely interconnected.

The above observation may be applicable more generally to the flow of incompatible polymer blends, e.g., Han et al.[21] show the η vs. $\dot{\gamma}$ plot for polystyrene/poly(methyl methacrylate) blends at 200°C, which is in qualitative agreement with our observations.

In the past, various schemes were applied for predicting the viscosity of the blend from the properties of the pure components.[22–26] An interesting method of master curve construction was recently proposed[27] for polypropylene–polyethylene blends. The scheme worked very well for that system at T = 180–200°C, but, due to the nature of the viscosity curves obtained in this study, it could not be used for our blends.

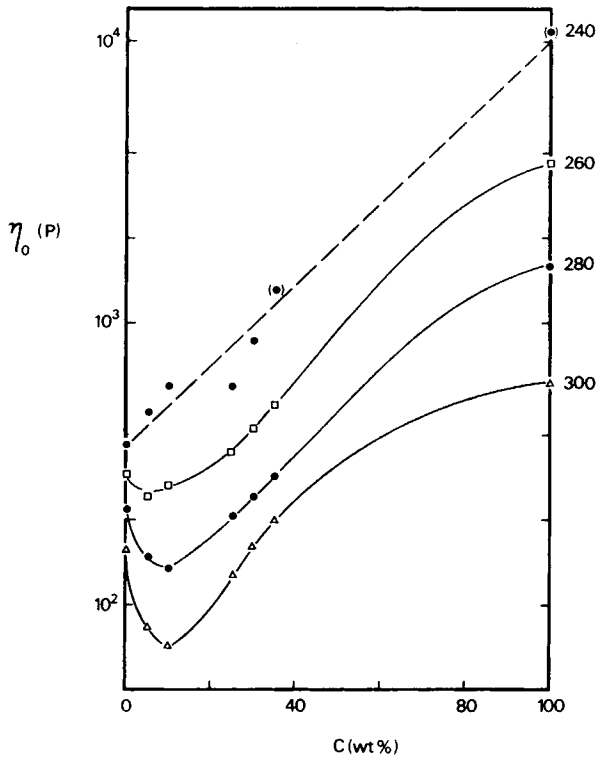

Fig. 14. Zero shear viscosities at four temperatures indicated vs. PA content. The points in parenthesis are from extrapolation.

As mentioned above, the ICR data were found to be only slightly affected by the capillary entrance and exit pressure drop. As a result, no corrections were made for these effects. Similarly, the effects of shear heating were neglected in these calculations.

The most significant difference between RMS and ICR results is that almost 30% higher values of η at 280°C are obtained in the capillary for B 2/1–B 2/4. At 300°C, the difference was smaller. This effect could not be attributed to shear crystallization,[28] which was observed by us only at 280°C for $\dot{\gamma} \geq 6 \times 10^4$ s^{-1}. Qualitatively, similar behavior was observed by Shih[29] and Kann and Shaw.[12] In their case, the depression of η by the addition of a small amount amount of the second polymer was very large in capillary flow, but virtually nonexistant[12] in other rheological tests. The authors[12,29] explain the phenomenon by the melt slip mechanism. Careful examination of the capillary and RMS dynamic mode flow patterns is being conducted to explain the observed behavior of the PET/PA blends.

Activation Energy of Flow, E_η

The values of this parameter for various systems are listed in Table III and shown in Figure 13. A comparison between the determined values and those reported in the literature for the pure components is given in Table V. It can be seen that E_η for PET from both RMS and ICR seems to be low in comparison

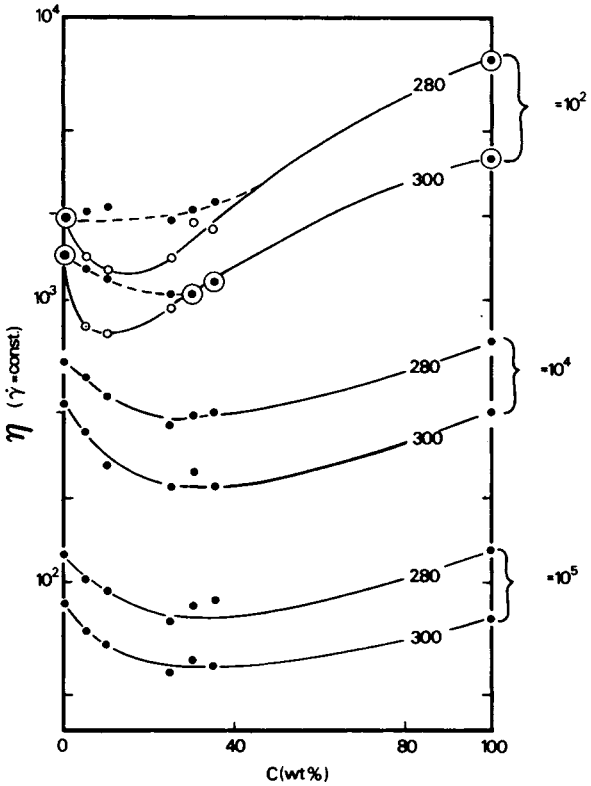

Fig. 15. Viscosities at constant rate of shear $\dot{\gamma} = 10^2$, 10^4, and 10^5 (s^{-1}) and at 280°C and 300°C vs. PA content. (●) ICR; (○) RMS; (⊙) both ICR and RMS.

with the literature values. The value for PA 42 agrees quite well with Westover's[33] result, but that obtained for PA 101 again seems to be on the low side. The difference is probably due to correcting for thermal degradation effects prior to calculation of E_η. Since all the samples underwent the same treatment, it is expected that the relative values of E_η are correct.

The E_η vs. c dependence, shown in Figure 13, tends to support the model proposed above for the flow of blend melts. The rapid initial increase of E_η is an indication of a sharp growth of the volume of the flow element.[34] The value of E_η seems to be fairly stable at higher concentrations.

TABLE IV
The Overall Activation Energy of Degradation for PET and PA

PET			PA		
E_D (kcal/mol)	Ref.	Comment	E_D (kcal/mol)	Ref.	Comment
30 ± 2	This work		47 ± 2	This work	PA 42
32	14		11 ± 2	This work	PA 101
29–41	16	Depending on type of catalyst	14–42	15	At 310–320°C
44	19	Calculated for T > 285°C	26, 41	17	Below and above 300°C, resp.
			30–65	18	

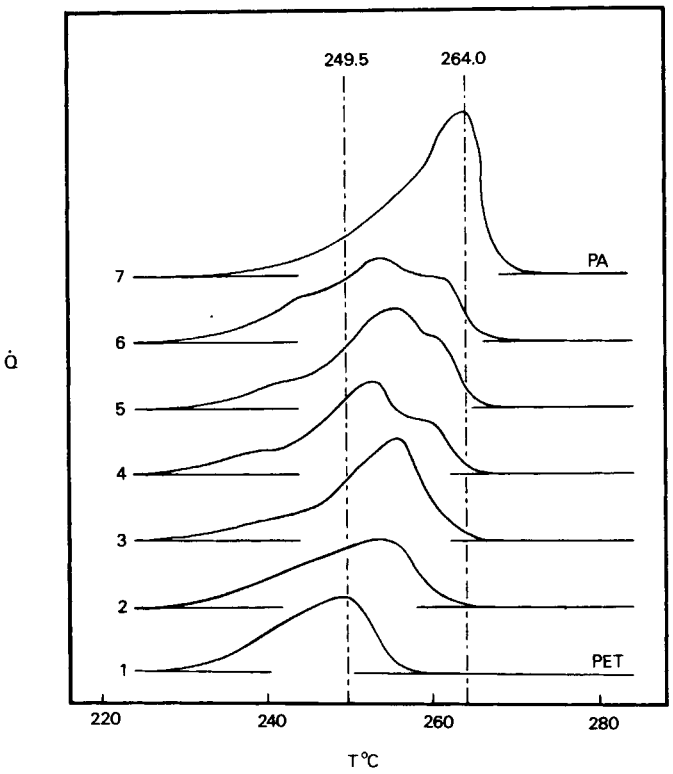

Fig. 16. DSC curves, samples numbered as in Figure 2, curves displaced vertically, vertical lines indicate T_m of pure polymers.

Composition Dependence of η

For homologous polymers, the log-additivity rule is generally accepted:

$$\log \eta_m = \sum c_i \log \eta_i \tag{5}$$

where η_i and η_m refer to viscosities of the pure components and their mixture, respectively, and c_i is the weight concentration of ingredient i. Recently,[35] another dependence

$$\eta_m^\alpha = \sum c_i \eta_i^\alpha \tag{6}$$

was proposed, where α is an adjustible parameter for the system. The relation, with $\alpha = 0.01$–0.57, was found to be valid for mixtures of homologous polymers of widely different chemical composition. In Figure 14, eqs. (6) and (5) with $\alpha < 0.2$ would define a straight line connecting the two pure polymers data points. For increasing α, eq. (5) would predict an upward curvature, i.e., in a direction opposite that indicated by the experimental results. It can be shown that the theoretically predicted dependence is symmetrical with regard to concentration.

For viscosities of nonhomologous polymer blends a series of empirical and semitheoretical relations have been proposed.[13,22–26,36] An interesting extension of Heitmiller et al.[37] approach was recently published by Lin.[38] The multiple sheath-core flow streams model in the capillary is hardly a realistic representation of polymer blend behavior, but it provides a reasonable means for interpretation

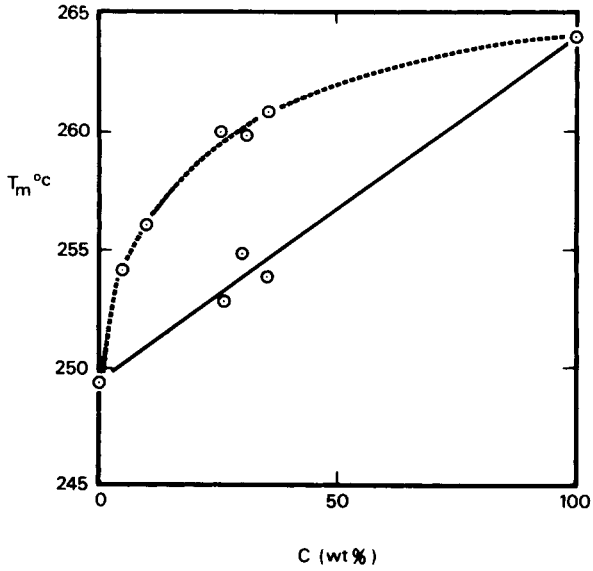

Fig. 17. Melting points (°C) (data from Fig. 16) as a function of PA content.

of the deviation of η_m from that predicted by eqs. (4) and (5). For a binary system[38]

$$1/\eta_m = \beta \sum c_i/\eta_i \tag{7}$$

where $\beta > 1$ represents the measure of interaction between the two phases. If $\beta = 1$, then the Heitmiller relation is recovered; if β is increased, then the negative deviation from log-additivity rule of the relation η_m vs. c deepens. Provided that the structure and properties of the interface do not change with c, eq. (7) should give a reasonable description. Unfortunately, in most of the polymer

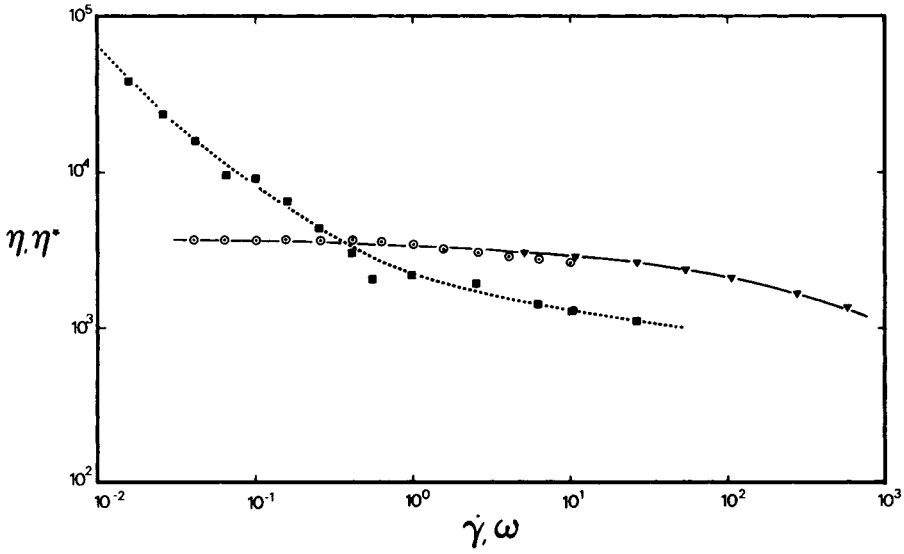

Fig. 18. Viscosities of B 2/4 at 280°C loaded at 280°C, 6-min soak (■) and at 290°C, 3-min soak (⊙); (▼) ICR.

TABLE V
Activation Energy of Flow for PET and PA

PET			PA		
E_η (kcal/mol)	Ref.	Comment	E_η (kcal/mol)	Ref.	Comment
9	This work	Zero shear	28	This work	PA 42
11	This work	$\dot{\gamma} = 10^3$	5	This work	PA 101
23.5	30	265–285°C	23.9	7	$10^5 < \sigma_{12} < 10^7$
19–34	31	Mol wt dependent	15	33	$M_n = 1.8 \times 10^4$
13.5	32		28.5	33	$M_n = 3.4 \times 10^4$
19	14				
21.1	19	275–295°C			

blends, this is not true. As in classical emulsions, phase inversion and partial solubilities complicate the behavior.[39,40]

Comparing the viscosity dependence predicted by eq. (7) with the results presented in Figures 14 and 15, one can postulate that a reason for η_0 to go through a sharp minimum must be some change in the liquid structure, which occurs at some low concentration: c^* = 5–10 wt % of PA (viz., Fig. 14). The minimum is not visible at 240°C, where PA crystallizes from the melt. On the other hand, as seen in Figure 15, for η ($\dot{\gamma}$ = const), the transition concentration c* seems to increase with $\dot{\gamma}$. In this regard, the difference in behavior of η ($\dot{\gamma} = 10^2$) with c observed in RMS and ICR measurements can be explained by differences in the phase structure of the blends in the two different flow geometries. It should be noted that this difference is observed only for some midrange concentrations c = 5–20%. In ICR and in RMS, the structures seem to remain relatively constant in the full range of investigated $\dot{\gamma}$ for each instrument, with the "slip factor" β being lower for the first than for the second instrument.

Melting Temperatures

The variation of T_m with c is shown in Figures 16 and 17. A comparison of T_m for the pure components is given in Table VI. It can be seen that the results of this work compare quite well with the reported values. Now, regarding the blends, the situation appears to be more complex: there seems to be two different types of melting points both of which depend on c. In the similar system,

TABLE VI
Melting Temperatures for PET and PA

PET			PA		
T_m (°C)	Ref.	Comments	T_m (°C)	Ref.	Comments
249.5	This work		264	This work	
249.3	28	Remelt	266	7	Mol wt = 14,000
249.5	28	Shear crystallized	259–269	41	Review
250 ± 1	42	Read from Figure 2, Ref. 42	268.5	44	Annealed
248	43	Read from Figure 2, Ref. 43	261.5	44	Not annealed
243	44	Slowly crystallized			

PET—polycaprolactam, the authors[42,43] reported very small (if any) variation of T_m with c. A decrease by no more than 6°C of the polycaprolactam peak and no change in that for PET was reported by Garg et al.[42] whereas Dimov et al.[43] suggested a slight shift in the position of the PET peak, explained by the postulated ester exchange reaction between the two polymers.

Judging from the results reported in Figures 16 and 17, PET/PA blends behave quite differently. Here the effect of polyamide addition is very strong, and obviously two different types of crystals are being formed. Their nature is being studied in detail.

Association

In Figure 18, the dynamic and steady state viscosities at 280°C are shown for the sample sample. Clearly two different types of rheological behavior are observed: the upper curve with a yield stress and the lower, showing the normal behavior. The difference is the result of employing a different initial temperature of the test fixtures while loading the sample. As can be seen in Figure 16, the base line for the sample B 2/4 is reached at $T < 270$°C, and even for pure PA, at about 275°C. Since the samples measured in DSC and RMS are the same, one is forced to postulate intermolecular associations in the blends. The phenomenon seems to be limited to high PA content samples only. The associations are apparently destroyed at $T = 285$–290°C.

Associations between PET and polycaprolactam macromolecules can be deduced from the infinite dilution viscosities.[45] Therefore, it seems reasonable to expect the occurrence of this phenomenon in PET—PA systems.

CONCLUSIONS

The rate and the activation energy of the thermal degradation of PET—PA blends are larger than expected from the simple additivity rule. The data for pure polymers agree quite well with those from the literature. The viscosity vs. rate of shear data suggest a mechanism of flow in which the droplets of PA dispersed in the PET matrix can be deformed at relatively low shear stress $\sigma_{12} = 10^3$ (dynes/cm^2). Only when the σ_{12} or $\dot{\gamma}$ is increased further by 1.5–2 decades, the normal transition into a "power-law" flow is observed. Thus, two step deviation from the Newtonian behavior makes it impossible to reduce the dependencies into a single master flow curves. Excellent agreement has been obtained between the rotational rheometer η vs. $\dot{\gamma}$ and η^* vs. ω results. Unfortunately, for samples containing $5 \leq c$ (wt % PA) ≤ 30, the ICR and mechanical spectrometer measurements yield different values of η, indicating a different flow mechanism in the two rheometers. The η vs. PA concentrations dependencies pass through a shallow minimum. The form of the dependencies pass through a shallow minimum. The form of the dependence suggests partial compatibility between the ingredients. This can be also deduced from the optical observations, the concentration dependence of T_m, and the yield stress observed for the blends at $T \leq 285$°C, i.e., well above T_m. It very well may be that the compatibility is a result of partial transesterification. This reaction seems to be more likely in the PET/PA than PET/polycaprolactam system. If this is true, then the former system should lead to more interesting commercial properties.

The authors are indebted to Mr. P. Sammut from the College Ahuntsic and Dr. H. P. Schreiber from Ecole Polytechnique (both of Montreal, Quebec) for their help in the preparation of the blends.

References

1. *Polym. News*, **7**(2), 86 (1981).
2. M. Shen and H. Kawai, *AIChE J.*, **24**(1), 1 (1978).
3. T. Alfrey, Jr., and W. J. Schrenk, *Science*, **208,** 813 (1980).
4. D. R. Paul and J. W. Barlow, *J. Macromol. Sci., Rev. Macromol. Chem.*, **C18**(1), 109 (1980).
5. J. Roovers, *Meth. Experim. Phys.*, **16C,** 275 (1980).
6. R. Simha, paper presented at the First IMRI Mini-Symposium on Phase Equilibria in Polymeric Systems, Montreal, 1980, NRCC Spec. Ed. 1982, L. A. Utracki, Ed.; *Polymer Eng. Sci.*, **22,** 74 (1982).
7. P. Parrini, D. Romanini, and G. P. Righi, *Polymer*, **17,** 377 (1976).
8. C. Macosko and J. M. Starita, *SPE J.*, **27,** 38 (1971); F. G. Mussatti and C. W. Macosko, *Polym. Eng. Sci.*, **13,** 236 (1973).
9. L. A. Utracki, Z. Bakerdjian, and M. R. Kamal, *J. Appl. Polym. Sci.*, **19,** 481 (1975).
10. L. A. Utracki, Z. Bakerdjian, and M. R. Kamal, *Trans. Soc. Rheolog.*, **19,** 173 (1975).
11. R. M. Schulken, R. H. Cox, and L. A. Minnick, *J. Appl. Polym. Sci.*, **25,** 1341 (1980).
12. R. Kann and M. T. Shaw, paper D8, presented at the 52nd annual meeting of the Society of Rheology, Williamsburg, Virginia, Feb. 23–25, 1981.
13. H. van Oene, in *Polymer Blends*, D. R. Paul and S. Newman, Eds., Academic, New York, 1978, Vol. 1, Chap. 7.
14. I. Marshall and A. Todd, *Trans. Faraday Soc.*, **49,** 67 (1953).
15. S. Straus and L. A. Wall, *J. Res. Nat. Bur. Std.*, **60,** 39, (1958); **63A,** 269 (1959).
16. H. Zimmerman and N. T. Kim, *Polym. Eng. Sci.*, **20,** 680 (1980).
17. E. P. Krasnov and L. B. Sokolov, *Vysokomol. Soed., Khim. Svoistva*, **1964,** 275 (1964).
18. I. J. Goldfarb and A. C. Meeks, AFML-TR-68-347. Part I (1969).
19. Z. Kembłowski, M. Michniewicz and J. Torzecki, *Rheology*, Proc. Intl. Congr. Rheol., G. Astarita, G. Marrucci, and L. Nicolais, Eds., Plenum, New York, 1980, Vol. 3, pp. 159.
20. Viz., e.g., L. A. Utracki, *J. Polym. Sci., Polym. Phys. Ed.*, **12,** 563 (1974).
21. C. D. Han, K. U. Kim, J. Parker, N. Siskovic, and C. R. Huang, *Appl. Polym. Symp.*, **20,** 191 (1973).
22. K. Maciejewski and R. G. Griskey, *Society of Plastics Engineers, 32nd Ann. Techn. Conf., Techn. Papers*, **20,** 23 (1974).
23. M. Kasajima, *Rheology Kondankai Yoshi*, 1 (1974).
24. M. Kasajima, *Bull. Coll. Eng. Hosei Univ.*, **15,** 1 (1979).
25. A. Kassa, W. E. Dreval, M. L. Kierbier, and I. K. Borisienkova, *Izv. Vys. Ucheb. Zovod., Khim. Khim. Techn.*, **22,** 1500 (1979).
26. J. F. Carley, *SPE, Techn. Reg. Conf. Plast. Progr. Proc.*, May 5–8, 1980, Techn. Papers, 285.
27. N. Alle and J. Lyngaae-Jørgensen, Rheol. Acta, **19,** 94 (1980).
28. P. D. Griswold and J. A. Cuculo, *J. Polym. Sci., Polym. Phys. Ed.*, **15,** 1291 (1977).
29. C. K. Shih, *Polym. Eng. Sci.*, **16,** 11 (1976).
30. S. Kawai, Y. Ichihara, H. Narukawa, and H. Nakayasu, *Nippon Kagaku Kaishi*, **1979**(10), 1371 (1979).
31. E. M. Aizenstein, B. W. Pietuchov, *Khim. Volok.*, **4,** 20 (1964).
32. D. R. Gregory, *J. Appl. Polym. Sci.*, **16,** 1479 (1972).
33. R. F. Westover, in "*Processing of Thermoplastic Materials*, E. C. Bernhardt, Ed., Reinhold, New York, 1959.
34. L. A. Utracki, *J. Macromol. Sci., Phys.*, **B18,** 725 (1981).
35. S. F. Christov, I. I. Skorokhodov, and Z. V. Shuraleva, Vysokomol Soed., **A20,** 1699 (1978).
36. B.-L. Lee and J. L. White, *Trans. Soc. Rheol.*, **19,** 481 (1975).
37. See Ref. 100 in Ref. 13.
38. C.-C. Lin, *Polym. J.*, **11,** 185 (1979).
39. See Refs. 92, 112 in Ref. 13.
40. K. Dimov, M. Savov, and J. Georgiev, *Acta Polym.*, **31,** 394 (1980).

41. H. W. Starkweather, Jr., in *Nylon Plastics*, M. I. Kohan, Ed., Wiley, New York, 1973, Chap. 9.
42. V. Garg, C. L. Nagendra, A. Misra, V. Chandhary, and D. S. Varma, *Angew. Makrom. Chem.*, **90,** 57 (1980).
43. K. Dimov, M. Savov and J. Georgiev, *Angew. Makromol. Chem.*, **84,** 119 (1980).
44. J. P. Bell and T. Murayama, *J. Polym. Sci., Part A-2*, **7,** 1059 (1969).
45. J. Repka, A. Marcivčin, and A. Pikler, *Chem. Vlakna*, **23,** 4 (1973).

Received April 3, 1981
Accepted November 20, 1981